A Battery-less BLE IoT Motion Detector Supplied by 2.45-GHz Wireless Power Transfer

Rémi Dekimpe, Pengcheng Xu, Maxime Schramme, Denis Flandre and David Bol
ICTEAM Institute, Université catholique de Louvain, 1348, Louvain-la-Neuve, Belgium
Email: {remi.dekimpe,david.bol}@uclouvain.be

***Abstract*—Wireless power transfer (WPT) is a possible way to achieve cheap, rapid and large-scale deployment of battery-less IoT smart sensors. However, the key challenge in designing WPT-supplied smart sensors is to ensure that the harvested power is higher than the consumed power in presence of strong WPT path loss. This paper presents the design and optimization of a smart sensor supplied by 2.45-GHz RF power and performing infrared-based motion detection and Bluetooth Low Energy (BLE) communication. The full system (RF energy harvester, power management, sensor transducer and interface, control, data processing and wireless transmission) is implemented using low-power off-the-shelf components. In the sensing sub-system, low average power is achieved using efficient duty-cycling of the analog front-end. In the harvesting sub-system, architecture choice and design of the matching network and rectifier circuit allow to optimize the total power harvesting efficiency (PHE). The implemented smart sensor can operate reliably with an incident RF power as low as -10.9 dBm. The sensing sub-system exhibits an average power of 4.3 μW and a maximum number of transmitted event packets of 60 packets per hour.**

I. Introduction

In the near future, thanks to the Internet of Things (IoT), data gathered by hundreds of billions of sensors distributed in our environment will help us to create more efficient systems that can do more with less resources. Examples are smart homes and smart buildings equipped with air quality, occupancy or temperature tracking system.

To ensure fine-grained monitoring of each room and space, those distributed sensor networks can include up to hundreds of sensor devices in a single multistory building. The installation of such network is therefore not only constrained by the cost of a single device, but also quite significantly by the deployment cost including the wiring infrastructure required for powering and/or communicating with each of them. The communication problem can easily be solved by relying on wireless protocols designed for sensor systems such as long-range LPWAN (LoRa, SigFox, NB-IoT) or short-range networks (ZigBee/802.15.4, Bluetooth LE). The power issue however proves to be trickier. One straightforward solution is supply the smart sensors with primary batteries but this raises other issues in terms of maintenance (battery replacement) and environmental impact (battery ecotoxicity) [1]. The ideal solution would be to rely on energy scavenging, that is, a way to continuously retrieve some energy from the environment to recharge a storage element. However, achieving balance between the fluctuating scavenging power and consumed power in such system while maintaining sufficient quality of service (QoS) is a challenging task. Therefore, wireless power transfer has emerged as an interesting alternative to achieve cheap and large-scale deployment of battery-less IoT smart sensors, as it allows continuous power harvesting on the sensor side.

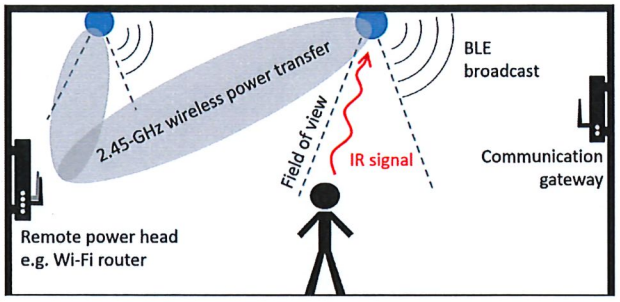


Fig. 1. Battery-less presence tracking room infrastructure with wireless power transfer. The sensor system (in blue) harvests RF power, detects motion via infrared light and uses BLE to transfer information wirelessly.

Within this study of WPT-supplied IoT smart sensors, we focus on the design of an infrared motion detector as a use case. The principle is that variations in the amount of human-emitted infrared light in the sensor field of view can be used as an indicator of human presence. As shown in Fig. 1, we can thus track the room occupancy by fixing several such detectors on the ceiling and transmitting this occupancy information wirelessly to a gateway. This can serve various purposes such as intruder detection, lighting control or HVAC regulation. For the data transmission, many low-power communication standards have been developed recently, typically for IoT devices. We selected Bluetooth LE (BLE) because as a short-range communication scheme it offers much lower energy per packet transmission compared to LPWAN [2]. BLE-connected sensors for smart buildings are already commercialized by companies such as Gooee or bGrid. For the WPT, we use remote power heads that can transmit directed beams of RF power towards the sensors. Those remote power heads could be embedded in e.g. Wi-Fi routers that are already widely deployed in buildings.

However, due to the equivalent isotropic radiated power (EIRP) regulations for the remote power heads and the WPT path loss, the incident RF power at the sensor side will be very limited. In this paper, we thus focus on designing a battery-less WPT-supplied IoT smart sensor that requires minimum RF input power to ensure correct motion detection.

To balance the power consumption against potential reduction of the quality-of-service (QoS), we perform power modeling of the different blocks where it is applicable. Section II emphasizes the power design constraints by linking incident RF power, energy harvesting efficiency and power consumption aspects. Comparison with existing designs is also addressed. In Section III, we give an overview of the system architecture. Section IV describes the design of the power management unit, including the selection of the storage element and of the system supply voltage. In Section V, we detail the power optimization of the sensing sub-system with duty-cycling of the sensor interface. Section VI shows the architecture of the RF energy harvester with emphasis of the relationship linking the different blocks to the overall efficiency of the harvesting subsystem. Prototype fabrication and system evaluation results are provided in Section VII.

II. Energy Harvesting Power Budget

In a battery-less system, one needs to balance harvested power, resulting from the incident power from the environment and the efficiency of the harvester, with the required power needed to supply the system. The RF incident power depends both on the power emitted by the remote power head and its distance to the sensor system. In Europe, the legal maximum emitting power of an RF source in the ISM band (2.45 GHz) is +24 dBm. Using a directional antenna array, it is possible to receive -15 dBm up to 4-5 meters from the source [3]. This incident power needs to be converted to a stable DC voltage to supply the sensing sub-system. This conversion is done, at the expense of some power losses, by the RF energy harvester and the power management unit. Finally, the combination of input power and harvesting efficiency sets the maximum average power that can be delivered to the system.

The performance of the RF energy harvester (RFEH) is best defined by its power harvesting efficiency (PHE), i.e. the ratio between the input incident RF power and the average output power, which is also equal to the product of the power extraction efficiency and the power conversion efficiency (PCE) [4]. The PHE of an energy harvester always depends on the incident input power and frequency. In Fig. 2, the harvested power available for the system is given for different PHE levels. State-of-the-art (SOA) RFEHs based on custom integrated circuits can achieve a peak PHE around 30% [5]–[10]. Among the commercially-available RFEHs, the P2110B and P1110B from Powercast are single-package RF energy harvesting solutions [11], [12], respectively with and without embedded energy storage charger (such as a secondary rechargeable battery). Without energy storage, the P1110B shows better efficiency. However, if used alone, the harvested power should be matched not to the average system power but to the worst-case system peak power (e.g. during BLE packet transmission). The PHE curve of the P2110B only demonstrates high efficiency at high input power (above -5 dBm), which significantly limits the WPT range.

Most RFEHs are designed for sub-GHz WPT to limit the path loss. In the proposed system, we focus on 2.45 GHz WPT

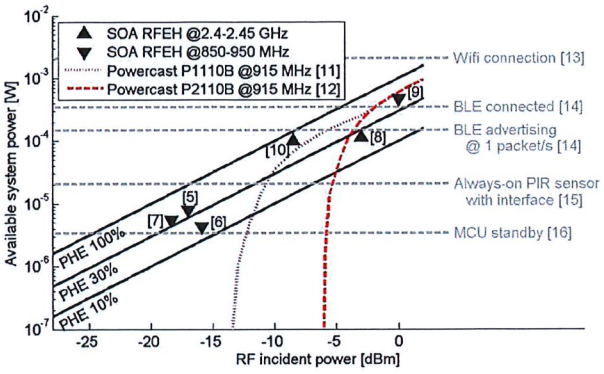


Fig. 2. RF energy harvesting power budget. The power harvesting efficiency (PHE) links the incident power to the available average power for the system. Horizontal lines indicate typical power consumption related to the relevant tasks of our target system.

for compact antennas and to reuse existing WiFi routers or master BLE devices as remote power heads. This comes at the cost of a more complicated design due to an increased impact of parasitics and therefore reduced PHE [10], as observed from the lack of data points in Fig. 2 at low RF incident power for 2.45 GHz WPT.

The harvested power available for the system determines which tasks can be performed or how they can be performed. At -15 dBm, the available power is a few μWs. In Fig. 2, typical power consumption values are shown for various tasks of a sensor system relevant to our goals, as extracted from technical references [13]–[16]. From this graph, we can see that the minimum incident RF power for a given PHE is set by the system task that needs to be executed.

III. System Architecture

Fig. 3 shows the proposed architecture for the battery-less motion detection sensor system. The harvesting sub-system interfaces the antenna and generates a regulated supply voltage for the sensing sub-system, which performs the motion detection from the infrared signals and transmits wirelessly the room occupancy information. In the harvesting sub-system, the RFEH harvests the RF power and rectifies it to an unregulated DC voltage. From this voltage, a power management unit (PMU) generates the appropriate regulated supply voltage. It also uses an energy storage element that stores the excess energy when it is not immediately needed by the sensing sub-system, or provides excess power when the sensing sub-system consumes more power than harvested power. The sensing sub-system is composed of a passive infrared (PIR) transducer connected to a sensor interface that amplifies and filters the signal. A microcontroller (MCU) with embedded ADC digitizes this signal. It also processes the acquired data to detect motion, by comparing the difference between sucessive samples with a predefined threshold. When a motion event is detected it triggers BLE transmission with a radio transceiver. In the proposed system, we selected a wireless MCU combo with embedded BLE transceiver. Let us mention

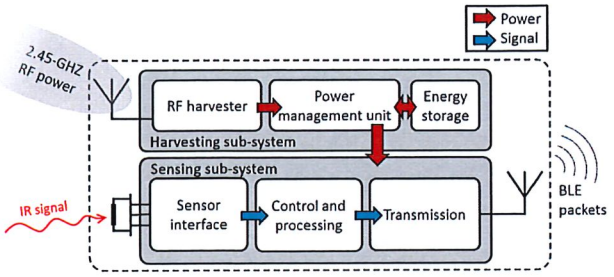


Fig. 3. System architecture. The harvesting sub-system converts RF power to a stable supply voltage. The sensing sub-system uses this supply to perform the motion detection task.

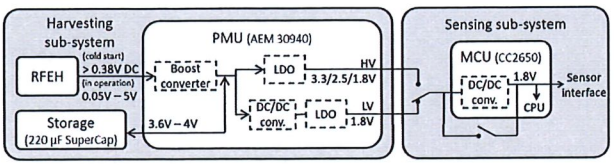


Fig. 4. Schematic of the power management across harvesting and sensing sub-systems. The DC output voltage of the RFEH is boosted to charge the SuperCap. Two paths (HV and LV) allow generating appropriate supply voltage to the sensing sub-system. The DC/DC converter of the MCU converts the voltage to 1.8V if necessary.

that local data processing on the smart sensor allows reducing the communication packet rate by only transmitting detected events instead of raw data, thereby significantly saving system power [17].

IV. Power Management

Smart power management is paramount for a system in which each μW has its importance. In this section, we explain and quantify how power is converted from the RFEH output to the sensing sub-system supply through the power management unit and storage element. It is the opportunity to show how thorough evaluation of the efficiency of each block present in the PMU can help choosing the most appropriate supply strategy. The choice of the storage element is also discussed.

Fig. 4 shows the power management schematic across harvesting and sensing sub-systems. The main power management unit (PMU) is the AEM30940 from e-peas semiconductors [18]. It extracts power from the low unregulated RFEH output voltage and slowly charges an energy storage element, both using an input/output voltage regulated boost converter. The stored energy is then converted to a stable voltage for supplying the sensing sub-system. The AEM can be configured to accommodate for different storage element types (Li-Ion battery, thin-film battery, super- or conventional capacitor) and supply different voltages (1.8, 2.5 or 3.3 V). Two different paths can be used to provide the supply voltage : High Voltage (HV) with a single LDO regulator, or Low Voltage (LV) with a DC/DC converter and an LDO regulator. The selected wireless MCU combo is the CC2650 from Texas Instruments. It has an internal DC/DC converter that allows operation between 1.8 and 3.8 V. At 1.8 V, it is more efficient to by-pass this converter [16].

In order to choose the best configuration for the power management across the PMU and the MCU, it is necessary to take into account the converting efficiency of the different stages. Figure 5 shows the power losses in four different configurations. The total height of each bar corresponds to the harvested power that must be provided by the RFEH in order to reach a fixed output load power of 30 μW at 1.8 V, corresponding to the power required for sensing and advertising BLE data (Fig. 2). The power losses in the voltage converters were measured for each component as the difference between their input and output power. From this graph, we see that the most efficient configuration is when the AEM30940 PMU directly provides a supply voltage of 1.8 V through the LV path, and the DC/DC converter of the MCU is therefore disconnected.

For the selection of the energy storage element, several factors need to be taken into account: lifetime, energy capacity, number of charge cycles and self-discharge rate (see Table I). Because of their limited lifetime and maximum number of charge cycles, most chemical batteries, such as Lithium-Ion are not suited for this application. Conventional electrolytic capacitors usually show significant leakage currents which, given the low amount of available power, is not acceptable. The best trade-off is given by the super-capacitor (SuperCap) that offers longevity, limited self discharge and compact energy density. The capacitance value needs to be chosen so that the SuperCap can tolerate the most energy-demanding tasks while keeping a voltage that is high enough. The task that requires the most energy over a short period is the BLE transmission measured at 75 μJ per packet, with an average power of 12.5 mW for 6 ms. The SuperCap should therefore be able to provide 150 μJ in the worst case (when 2 events occur successively as will be discussed in Section V-C) when the voltage drops from 4 V, which is the rated voltage limit set by the AEM30940 PMU, to 3.6 V, which is the minimum voltage in its default configuration. Using

$$\Delta E = \frac{1}{2} C (V_{high}^2 - V_{low}^2) \quad (1)$$

where ΔE is the energy available from a capacitor with capacitance C when changing from a voltage V_{high} to a voltage V_{low}, we get that the capacitance of the storage element should be above 150 μF. In practice we selected cheap and ultra-compact 220 μF SuperCap, as the datasheet of the AEM30940 suggests this minimum capacitance value.

V. Sensing Sub-System

The sensing sub-system senses the infrared signal, processes the data to detect motion and transmits the occupancy information wirelessly. Fig. 6 shows the sensing sub-system architecture with the CC2650 wireless MCU combining processing and transmission functions.

The CC2650 MCU must periodically sample the analog sensor signal, process the data and control the wireless communication. To this end, we use the real-time clock (RTC) to

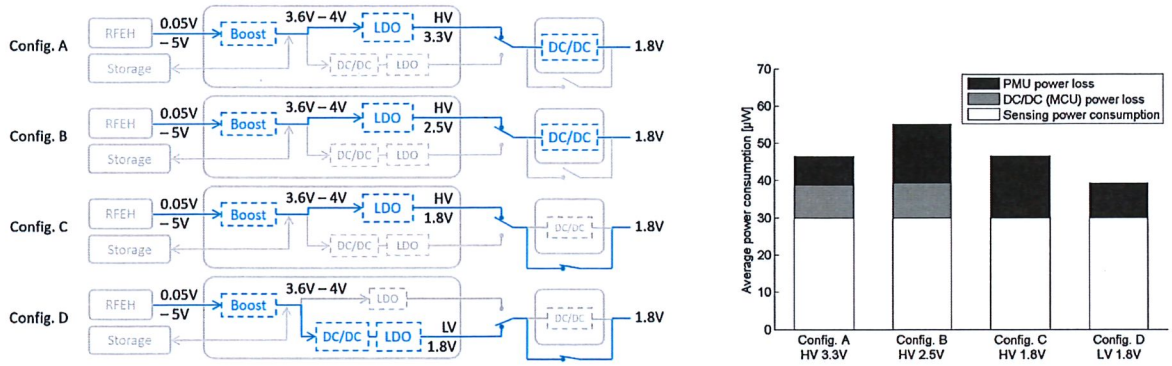


Fig. 5. Four possible power management configurations (left) and measured associated total power consumption (right). On this bar chart, the total height gives the required input power from the RFEH, the white part is the power to be delivered to the sensing sub-system circuits and the gray and black parts depicts the power management losses, as a function of the chosen power management configuration.

TABLE I
CHARACTERISTICS OF STORAGE ELEMENT TYPES [19], [20].

	Li-Ion battery	Super-capacitor	Electrolytic capacitor
Energy density [Wh/kg]	10-100	1-10	< 0.1
Lifetime [years]	3-5	> 10	> 25
Max. charge cycles	500-2000	> 500000	$\approx$ unlimited
Self-discharge [%/day]	< 0.5	< 20	> 100

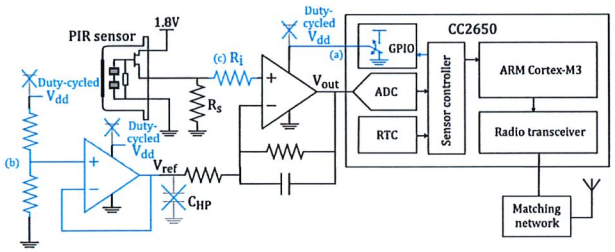


Fig. 6. Schematic of the sensing sub-system. Changes made for duty-cycling the sensor interface are highlighted in blue : GPIO supply switching (a), voltage reference (b) and amplifier input resistance (c).

wake up the sensor controller every 1 second, which triggers a digitization operation by the ADC. The sensor controller is a low-power co-processor embedded in the CC2650 MCU designed for efficient peripheral management. As this co-processor is capable of performing basic mathematical tasks, we also use it for simple motion detection by comparing the difference between two successive samples with a predefined threshold. If motion is detected, an interrupt request (IRQ) is sent to the CPU (Cortex-M3) to trigger a BLE event packet transmission.

The sensor transducer is a PIR sensor ZRE200GE from Zilog. This sensor requires an interface to amplify and filter the signal before it can be digitized. As detailed in the datasheet of the transducer [21] and in an application note from Texas Instrument [15], this can be done using an active non-inverting band-pass amplifier circuit built around an operational amplifier as shown in Fig. 6. In order to reduce the power consumption, we use an ultra-low-power amplifier (TLV8802 [22] from Texas Instrument). The output of the amplifier is connected to the ADC input of the CC2650 MCU for digitization.

The following sub-sections detail how we achieve ultra-low-power operation to meet the low power budget set by the energy harvester. In addition to 1.8 V operation discussed in the previous section, several solutions will be studied and experimentally quantified. Firstly, duty-cycling of the sensor interface allows to significantly reduce the power consumed by the sensor interface. A second improvement is the reduction of the power required for the PIR sensor while limiting the impact on the sensitivity. Finally, changing the wireless transmission strategy makes it possible to reach the expected power requirements.

A. Sensor interface duty-cycling

One approach for the reduction of power consumption is the power duty-cycling. This consists in switching back and forth between an active mode that allows to perform the task but consumes a large amount of power and a low-power sleep mode in which no operation is possible. The objective is to perform the task as quickly as possible to limit the time in active mode and save power in sleep mode. Thanks to its general purpose input/output (GPIO) pins with high-drive capability (4 or 8 mA), the sensor transducer and sensor interface can be powered directly from the CC2650 and therefore duty-cycling can be applied as shown in Fig. 6(a). The main constraint in applying this technique is the time required to switch from one mode to the other. In this analog circuit, this wake-up time is mainly due to the charge and settling time of nodes in the circuit. The most critical timings are the charge of the high-pass capacitor C_{HP}, the start time of the operational amplifier and the settling time of the sensor.

The charge time of the capacitor is proportional to the inverse of its cut-off frequency. Because the signal of the PIR has a low frequency (between 0.5 and 5 Hz), the charge time is on the order of 1 second. Considering a sampling frequency

of 1 S/s, the power reduction offered by duty-cycling with such a long charge time is not interesting. A solution is to replace this high-pass capacitor by a voltage reference (V_{ref}) set as close as possible to the DC voltage at the output of the PIR sensor. The voltage reference is built using a voltage divider and a voltage follower amplifier (Fig 6(b)). This solution works as long as the difference between those two voltages multiplied by the gain of the amplifier stays within the saturation limits. According to our measurements, a maximum difference (including resistor precision, temperature and illumination variations and device-to-device variations) smaller than 30 mV is observed. Considering a dynamic output voltage range of 1.8 V, this allows for an amplifier gain up to 60 V/V to avoid saturation. As the range of variations on the sensor output is around 1 mV and the resolution of the ADC is 2 mV, this gain is large enough. Because of the resistive voltage divider, this voltage reference circuit consumes a large amount of power when active (3 μW). However, duty-cycling makes it negligible in the total power consumption.

The starting time of the operational amplifier has been measured to be 4.5 ms. Before this period, the output of the interface does not provide any information on the sensor state as shown in Fig. 7. This therefore sets a limit on the minimum active time period and on the minimum duty-cycle percentage. The settling time of the PIR sensor is about 30 seconds which is too long to consider duty-cycling. The sensor therefore has to stay powered on at all times. In order to limit its continuous power consumption, we have to increas the biasing biasing R_s as will be discussed in Section V-B.

One additional problem that occurs when the power of the TLV8802 amplifier is cut off is that it loses its high impedance at the input pins. This means that the source resistance found in Section V-B is significantly reduced and the current increases to 2 μA. This can be solved by adding a large series resistance R_i of 8 MΩ as depicted in Fig. 6(c). This has no impact on the gain or signal-to-noise ratio (SNR) of the amplifier circuit during operation but limits the current when the amplifier is shut off.

The sensor interface can therefore be duty-cycled with an active period of 10 ms every 1 s. With a power consumption in active mode and in shutdown mode of 5.5 μW and 180 nW respectively, the average duty-cycled power is 235 nW. Unfortunately, duty-cycling the sensor interface also comes at the cost of waking up the sensor controller twice: once to activate the supply via the GPIO, and once to sample the data and turn off the GPIO. This increases the average power by 290 nW, which still pays back significantly when compared to the active mode power of 5.5 μW.

B. PIR sensor power-performance optimization

The part of the sensing sub-system that consumes most of the power is the PIR sensor. This power consumption can be modified by changing the R_s resistance connected between the source of the sensor and the ground. In order to avoid degrading the sensing performance and find an optimal resistance, we measured the power consumption and output SNR

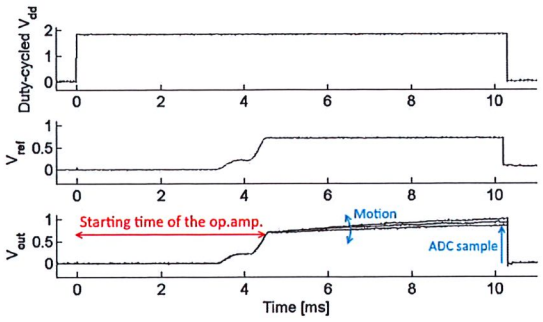


Fig. 7. Measured sensing sub-system signals when duty-cycling the sensor interface. Traces of the amplifier output for different samples are superimposed to show the effect of motion on the signal.

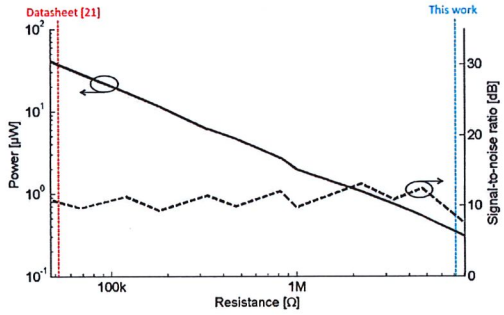


Fig. 8. Measured power consumption of the PIR sensor and output signal-to-noise ratio for different values of resistance between the source of the sensor and the ground.

of the sensor for various source resistance values (see Fig. 8). The power is dramatically decreased with higher resistance while the impact on the SNR is limited. The resistance value is therefore chosen as 8 MΩ, much higher than the value suggested in the datasheet (47 kΩ).

C. Asynchronous BLE transmission

Wireless transmission represents a significant part of the total power consumption. BLE broadcasting consists in sending data periodically at a chosen advertising interval in dedicated channels, not knowing if other devices are listening. While we can consider that the energy per packet is fixed, there are ways to modify this communication scheme to reduce the number of transmitted packets, and therefore the average power consumption. This can first be done simply by increasing the advertising interval, at the cost of a proportional increase in latency of the response to a motion. Generally speaking, broadcasting data periodically has the disadvantage of consuming large amounts of energy recurrently during the transmissions even if nothing happens in the sensor signal. To avoid this, an alternative strategy is to process the data locally and broadcast an information packet asynchronously only when an event is detected [17]. In our case, the events are when a motion starts or ends, which means that room occupancy changes. In this case, the average power consumption can

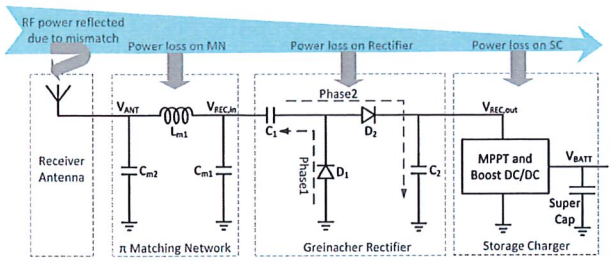


Fig. 9. Schematic of the RFEH.

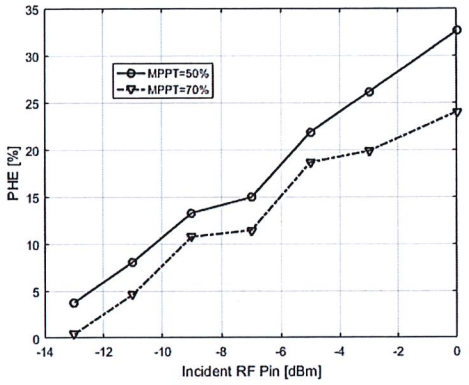


Fig. 10. Power harvesting efficiency of the RF energy harvester depending on the RF incident power for different MPPT configurations.

be kept at a minimum when nothing happens. However, the maximum average power consumption that we need to take into account in the power budget is when there is frequent occupancy changes in front of the sensor. To avoid transmitting nearly every second in such case, we can define the event corresponding to the end of motion as when no motion was observed for a given blackout period, e.g. 1 minute. This allows to fix a maximum transmission rate, while keeping short latency when new events occur. The disadvantage is that occupancy changes that are closer than the selected time duration cannot be distinguished, but this has little impact in the foreseen applications. Section VII will discuss how to set the motion blackout period depending on the available system power.

VI. RF ENERGY HARVESTER

A typical RF energy harvester system is usually composed of an antenna, an impedance matching network, an AC/DC rectifier and an energy-storage manager. The role of the matching network is to match the input impedance of the rectifier to the antenna impedance, usually 50 or 75 Ω. The total power harvesting efficiency (PHE) is the result of the power losses in these 3 stages. As illustrated in Fig. 9, four main sources of RF power losses in RFEH subsystem are to be considered: RF power reflected due to impedance mismatch, power loss on the matching network, power loss on the AC/DC rectifier and power loss the on storage charger. Therefore, the PHE can be described as:

$$PHE = \eta_{extract} \times PCE_{MN} \times PCE_{REC} \times PCE_{SC} \quad (2)$$

where PCE is the conversion ratio for each block, i.e. the respective ratio between input and output power, and $\eta_{extract}$ is extraction efficiency i.e. the ratio between the power transmitted to the matching network and the incident power.

As shown in in Fig. 4, the proposed RFEH is based on a receiver patch antenna printed on the PCB, a π matching network, a Greinacher rectifier and a storage charger. As explained in Section III, the storage charger is included in the AEM30940 PMU. It integrates maximum power point tracking (MPPT) and boost DC/DC converter.

Compared to the two-element L matching networks for which the quality factor Q is set by the source and load impedance, the three-element π network overcomes this disadvantage and can be used for narrow-band high-Q applications [23]. Additionally, tuning the C_{m2} capacitance in the π matching network can be used to compensate the parasitic capacitance of the rectifier diodes. The Greinacher doubler circuit schematic is represented in Fig. 9. During Phase 1, when the AC input voltage $V_{REC,in}$ is below the ground level and its absolute value is larger than the threshold voltage V_t of the diode D_1, a forward current is generated and flows from the ground to the matching network. The charges accumulate on capacitor C_1. During Phase 2, when the AC input voltage $V_{REC,in}$ is above the ground level and its absolute value is larger than the V_t of D_2, the diode D_1 turns off and D_2 turns on. The forward current flows from the input capacitor C_1 through the output diode D_2 to the output filter capacitor C_2. The output voltage of Greinacher rectifier $V_{REC,out}$ can influence its impedance and have further effect on PHE. By regulating the rectifier output voltage $V_{REC,out}$ with maximum power point tracking (MPPT) as done by the AEM30940 PMU, $V_{REC,out}$ is forced to be at a certain ratio of its open load output voltage to track the maximum PHE.

To size the matching network, we need to consider fixed input/output impedances. However, the rectifier input impedance varies with $V_{REC,in}$, which depends on the incident RF power. Therefore, the matching network efficiency significantly decreases at low incident RF power, when the rectifier impedance diverges from its nominal value, as shown in Fig. 10 and Fig.11. In this design, the matching network is sized at low rectifier impedance with high incident RF power (-5 dBm), because both the diode and PCB parasitic capacitors add up to C_{m1} and make the matching network hard to size at lower RF incident power with high rectifier impedance. We can also see in these figures that the lower MPPT ratio has a better PHE and larger available output power. This is explained by the fact that the rectifier impedance is lower with a lower rectifier output voltage $V_{REC,out}$. This configuration is closer to the nominal case since the fixed π matching network is sized at low rectifier impedance as mentioned above.

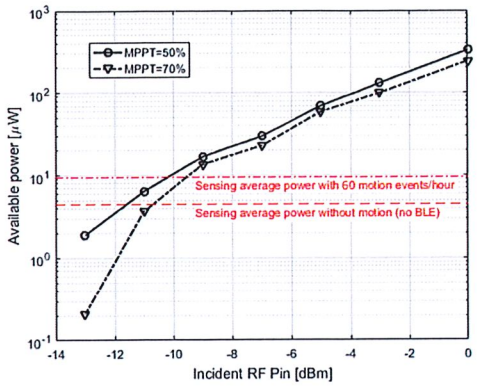


Fig. 11. Available output power from the RF energy harvester. The red lines show the power consumption of the sensing sub-system under different operating situations.

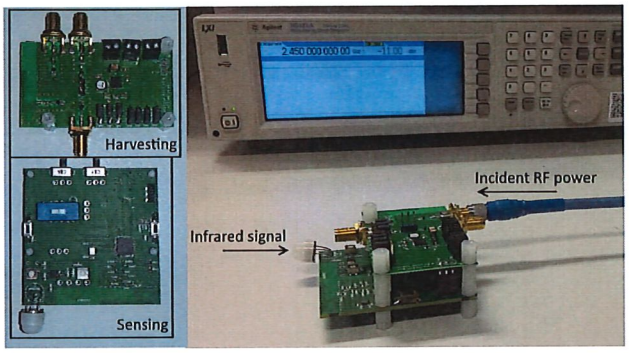


Fig. 12. PCB prototypes (left) and characterization setup (right).

VII. Prototyping and System Evaluation

Both harvesting and sensing sub-systems were prototyped in separate pluggable PCBs. The whole system was tested using an RF generator (Synthe MXG N5181A) connected with an SMA cable as input power source to characterize the minimum RF input power to ensure correct motion detection (see Fig.12). While the system requires a short initial burst of power at 0 dBm to cold-start the AEM30940 PMU, the system can work in regime with an incident power down to -11.9 dBm (without BLE motion events). The main measured performance metrics of the system are listed in Table II.

As explained in Section V-C, an asynchronous broadcast scheme is used for the wireless transmission. To limit the number of transmissions, a motion blackout period must be selected. A longer time will limit the number of transmissions but reduce the ability to distinguish occupancy changes that are closer in time. In order to meet the power budget, this blackout period can be found based on the available power from the energy harvester ($P_{harvest}$), the average power consumed by the sensing sub-system when no motion is observed (P_{sens}) and the energy required for the transmission of an event packet (E_{BLE}). Using those parameters, the minimum

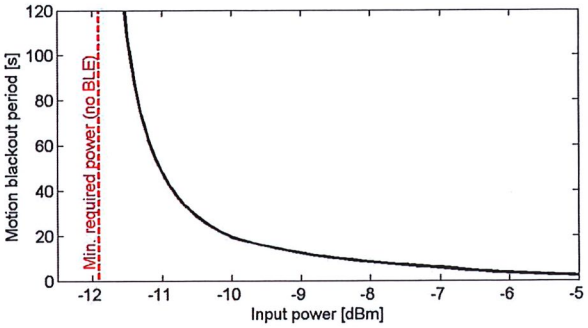


Fig. 13. Trade-off between input power and motion event duration.

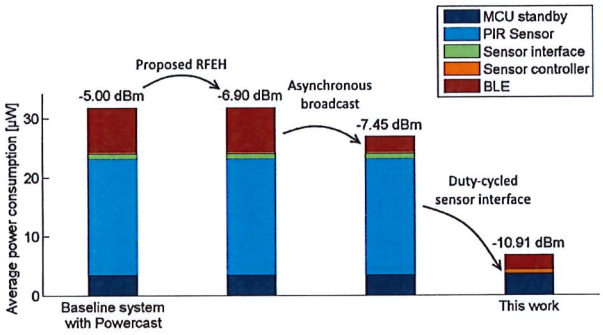


Fig. 14. Successive system optimization steps. Each bar corresponds to the power consumption of the sensing sub-system at some stage of the optimization. The numbers on top of each bar represent the minimum required incident RF power.

blackout period that can be selected is :

$$T = \frac{2 \times E_{BLE}}{P_{harvest} - P_{sens}}. \quad (3)$$

The denominator of the fraction can be understood as the power available for transmission after removing the average sensing power. The factor 2 is due to the fact that 2 packets can be sent consecutively if a new motion starts just after the end of the previous blackout period. Figure 13 shows the trade-off between the incident RF power and the minimum blackout period. The red dashed line represents the minimum incident power required to make the sensing sub-system work.

To summarize the power optimization steps performed on the system, Fig. 14 shows the average power consumption of the sensing sub-system and the corresponding minimum input RF power required. We see that the proposed RFEH allows to reduce the required power for an identical power consumption. Additionally, the different optimization steps performed on the sensing sub-system reduce the power consumption and therefore the minimum incident RF power as well. In total, the designed system offers a reduction of 6 dB (4 ×) in required incident power compared to the baseline case.

VIII. Conclusion

This paper investigated how to meet the power constraints set by the battery-less operation of a motion-detection sensor

TABLE II
MEASURED PERFORMANCE RESULTS.

Min. RF incident power (without motion)	-11.9 dBm
Min. RF incident power (with 60 events / hour)	-10.9 dBm
Average power consumption without motion	4.3 μW
BLE transmission energy per packet	75 μJ
Maximum motion detection distance	4 m
Motion detection false alarm rate	$<$ 0.06 / hour

system. In this system, it has been achieved by the implementation of an RFEH with descent PHE at lower incident power as well as the ultra-low-power consumption of the sensing sub-system. The RFEH alone operates with an incident RF power as low as -13 dBm and the power consumption of the sensing sub-system is 4.3 μW when there is no motion. By selecting a motion blackout period of 1 minute, the average power consumption raises to maximum 6.8 μW and the continuous operation of the smart sensor is possible down to -11 dBm of RF power incident to the RFEH.

ACKNOWLEDGMENT

The authors would like to thank Pierre-Antoine Haddad and Sarah Hautain for fruitful discussions with respect to RFEH modeling. This work was supported by the Brussels Institute for Research and Innovation (INNOVIRIS) under the COPINE-IoT project.

REFERENCES

[1] D. Bol, G. de Streel, and D. Flandre, "Can We Connect Trillions of IoT Sensors in a Sustainable Way ? A Technology/Circuit Perspective," *2015 IEEE SOI-3D-Subthreshold Microelectronics Technology Unified Conference (S3S)*, pp. 1–3, 2015, Invited speaker.

[2] M. S. Mahmoud and A. A. H. Mohamad, "A Study of Efficient Power Consumption Wireless Communication Techniques/Modules for Internet of Things (IoT) Applications," *Advances in Internet of Things*, vol. 6, no. 2, pp. 19–29, 2016.

[3] A. I. Akin, I. Stupia, and L. Vandendorpe, "On the effect of blockage objects in dense MIMO SWIPT networks," *ArXiv e-prints*, 2018.

[4] D. Bol, E. H. Boufouss, D. Flandre, and J. D. Vos, "A 0.48mm^2 5μW-10mW Indoor/Outdoor PV Energy-Harvesting Management Unit in a 65nm SoC based on a Single Bidirectional Multi-Gain/Multi-Mode Switched-Cap Converter with Supercap Storage," *2015 41st IEEE European Solid State Circuits Conference (ESSCIRC)*, pp. 241–244, 2015.

[5] M. Stoopman, S. Keyrouz, H. J. Visser, K. Philips, and W. A. Serdijn, "Co-Design of a CMOS Rectifier and Small Loop Antenna for Highly Sensitive RF Energy Harvesters," *IEEE Journal of Solid-State Circuits*, vol. 49, no. 3, pp. 622–634, 2014.

[6] G. Papotto, F. Carrara, and G. Palmisano, "A 90-nm CMOS Threshold-Compensated RF Energy Harvester," *IEEE Journal of Solid-State Circuits*, vol. 46, no. 9, pp. 1985–1997, 2011.

[7] S. Mandal and R. Sarpeshkar, "Low-Power CMOS Rectifier Design for RFID Applications," *IEEE Transactions on Circuits and Systems I*, vol. 54, no. 6, pp. 1177–1188, 2007.

[8] J. Masuch, M. Delgado-Restituto, D. Milosevic, and P. Baltus, "An RF-to-DC energy harvester for co-integration in a low-power 2.4 GHz transceiver frontend," *2012 IEEE International Symposium on Circuits and Systems (ISCAS)*, pp. 680–683, 2012.

[9] J. Wang, Y. Jiang, J. Dijkhuis, G. Dolmans, H. Gao, and P. Baltus, "A 900 MHz RF energy harvesting system in 40 nm CMOS technology with efficiency peaking at 47% and higher than 30% over a 22dB wide input power range," *2017 43rd IEEE European Solid State Circuits Conference (ESSCIRC)*, pp. 299–302, 2017.

[10] P.-A. Haddad, J.-P. Raskin, and D. Flandre, "Efficient passive energy harvesters at 950 MHz and 2.45 GHz for 100 μW applications in 65 nm CMOS," *2016 IEEE International Conference on Electronics, Circuits and Systems (ICECS)*, pp. 508–511, 2018.

[11] *P1110B 915 MHz RF Powerharvester Receiver*, Powercast, 2016.

[12] *P2110B 915 MHz RF Powerharvester Receiver*, Powercast, 2016.

[13] E. Dekel, "Low-power Internet connectivity over Wi-Fi," Texas Instruments, Tech. Rep., 2016.

[14] J. Lindh, C. Lee, and M. Hernes, "Measuring Bluetooth Low Energy Power Consumption," Texas Instruments, Tech. Rep., 2017.

[15] TI Designs, "Low-Power PIR Motion Detector With Bluetooth Smart and 10-Year Coin Cell Battery Life Reference Design," Texas Instruments, Tech. Rep., 2016.

[16] *CC2650 SimpleLink Multistandard Wireless MCU*, Texas Instruments, 2016, rev. B.

[17] D. Bol, "Ultra-Low-Power SoCs for Local Sensor Data Processing," *2018 IEEE International Solid- State Circuits Conference (ISSCC)*, 2018, Forum.

[18] *AEM30940 Highly-Efficient Regulated Dual-Output, Ambient Energy Manager for AC or TEG sources with optional primary battery*, e-peas, 2017.

[19] A. Gonzlez, E. Goikolea, J. A. Barrena, and R. Mysyk, "Review on supercapacitors: Technologies and materials," *Renewable and Sustainable Energy Reviews*, pp. 1189–1206, 2016.

[20] X. Jiang, J. Polastre, and D. Culler, "Perpetual environmentally powered sensor networks," *4th international symposium on Information processing in sensor networks*, p. 65, 2005.

[21] *ZMOTION Pyroelectric Sensors*, Zilog, 2017.

[22] *TLV8802/TLV8801 320 nA Nanopower Operational Amplifiers for Cost-Optimized Systems*, Texas Instruments, 2016, rev. A.

[23] C. Bowick, J. Blyler, and C. Ajluni, *RF Circuit Design*, 2nd ed. Newnes, 2008.